Journal of Nuclear Medicine, published on March 14, 2024 as doi:10.2967/jnumed.123.265997

Efficacy of [^{67}Cu]Cu-EB-TATE Theranostic Against Somatostatin Receptor Subtype-2–Positive Neuroendocrine Tumors

Fabrice Ngoh Njotu[1,2], Jessica Pougoue Ketchemen[1], Anjong Florence Tikum[1], Hanan Babeker[1,2], Brian D. Gray[3], Koon Y. Pak[3], Maruti Uppalapati[2], and Humphrey Fonge[1,4]

[1]Department of Medical Imaging, College of Medicine, University of Saskatchewan, Saskatoon, Saskatchewan, Canada; [2]Department of Pathology and Laboratory Medicine, College of Medicine, University of Saskatchewan, Saskatoon, Saskatchewan, Canada; [3]Molecular Targeting Technologies, Inc., West Chester, Pennsylvania; and [4]Department of Medical Imaging, Royal University Hospital Saskatoon, Saskatoon, Saskatchewan, Canada

β^--emitting ^{177}Lu-octreotate is an approved somatostatin receptor subtype 2 (SSTR2)–directed peptide receptor radionuclide therapy for the treatment of gastroenteropancreatic neuroendocrine tumors (NETs). However,^{177}Lu-octreotate has fast pharmacokinetics, requiring up to 4 treatment doses. Moreover, ^{177}Lu is less than ideal for theranostics because of the low branching ratio of its γ-emissions, which limits its SPECT imaging capability. Compared with ^{177}Lu, ^{67}Cu has better decay properties for use as a theranostic. Here, we report the preclinical evaluation of a long-lived somatostatin analog, [^{67}Cu]Cu-DOTA-Evans blue-TATE (EB-TATE), against SSTR2-positive NETs. **Methods:** The in vitro cytotoxicity of [^{67}Cu]Cu-EB-TATE was investigated on 2-dimensional cells and 3-dimensional spheroids. In vivo pharmacokinetics and dosimetry were studied in healthy BALB/c mice, whereas ex vivo biodistribution, micro-SPECT/CT imaging, and therapy studies were done on athymic nude mice bearing QGP1.SSTR2 and BON1.SSTR2 xenografts. Therapeutic efficacy was compared with [^{177}Lu]Lu-EB-TATE. **Results:** Projected human effective doses of [^{67}Cu]Cu-EB-TATE for male (0.066 mSv/MBq) and female (0.085 mSv/MBq) patients are tolerable. In vivo micro-SPECT/CT imaging of SSTR2-positive xenografts with [^{67}Cu]Cu-EB-TATE showed tumor-specific uptake and prolonged accumulation. Biodistribution showed tumor accumulation, with concurrent clearance from major organs over a period of 72 h. [^{67}Cu]Cu-EB-TATE was more effective (60%) at eliminating tumors that were smaller than 50 mm^3 within the first 15 d of therapy than was [^{177}Lu]Lu-EB-TATE (20%) after treatment with 2 doses of 15 MBq administered 10 d apart. Mean survival of [^{67}Cu]Cu-EB-TATE–treated groups was 90 d and more than 90 d, whereas that of [^{177}Lu]Lu-EB-TATE was more than 90 d and 89 d against vehicle control groups (26 d and 53 d), for QGP1.SSTR2 and BON1.SSTR2 xenografts, respectively. **Conclusion:** [^{67}Cu]Cu-EB-TATE exhibited high SSTR2-positive NET uptake and retention, with favorable dosimetry and SPECT/CT imaging capabilities. The antitumor efficacy of [^{67}Cu]Cu-EB-TATE is comparable to that of [^{177}Lu]Lu-EB-TATE, with [^{67}Cu]Cu-EB-TATE being slightly more effective than [^{177}Lu]Lu-EB-TATE for complete remission of small tumors. [^{67}Cu]Cu-EB-TATE therefore warrants clinical development.

Key Words: [^{67}Cu]Cu-EB-TATE; PRRT; SPECT/CT imaging; SSTR2; dosimetry

J Nucl Med 2024; 00:1–7
DOI: 10.2967/jnumed.123.265997

Received May 12, 2023; revision accepted Jan. 29, 2024.

For correspondence or reprints, contact Humphrey Fonge (humphrey.fonge@usask.ca) or Maruti Uppalapati (maruti.uppalapati@usask.ca).

Published online Mar. 14, 2024.

Neuroendocrine tumors (NETs) are a large group of diverse cancers of neuroendocrine origin that develop mostly within the gastrointestinal (66%) and pulmonary (31%) systems and account for 0.46% of malignancies of these systems (*1*). About 80% of NETs overexpress somatostatin receptor subtype 2 (SSTR2; 1 of 5 SSTRs [SSTR1–SSTR5]) (*2*). Using this receptor as bait has improved the diagnosis and treatment of NETs, primarily through the peptide receptor radionuclide therapy approach, which uses somatostatin analogs such as octreotate and octreotide labeled with radionuclides (*3*). So far, Health Canada, the Food and Drug Administration, and the European Medicines Agency have approved the use of β^--emitting ^{177}Lu-DOTA-Tyr^3-octreotate complex ([^{177}Lu]Lu-DOTATATE) for the treatment of metastatic or inoperable progressive gastroenteropancreatic NETs after PET image diagnosis with the short-lived [^{68}Ga]Ga-DOTATATE (^{68}Ga half-life [$t_{1/2}$], 67.71 min) (*4,5*).

The therapeutic effectiveness of [^{177}Lu]Lu-DOTATATE is attributed to the decay characteristics of its long-lived ^{177}Lu isotope ($t_{1/2}$, 6.65 d; β^-, 100%; mean β^--energy, 134 keV; maximum β^--energy, 497 keV), which gives its ionizing β^--emissions a tumor penetration depth of 2 mm, and the tumor specificity and high binding affinity of octreotate. Similarly, the short-lived ^{68}Ga is optimal for PET imaging, thus making it a theranostics pair with ^{177}Lu (*5*). However, a limitation in differential clearance exists with a short-lived radionuclide (^{68}Ga) to estimate dosimetry for a long-lived radionuclide (^{177}Lu), an important consideration as it allows for accurate prospective determination of peptide receptor radionuclide therapy dose at an optimal therapeutic index. Additionally, the short $t_{1/2}$ of ^{68}Ga could limit the sensitivity of the diagnostic, especially for lesions in organs with a high blood pool. This thus poses the need for a matched theranostics pair or, extraordinarily, a theranostic single.

Copper has 2 medical radionuclides, long-lived ^{67}Cu ($t_{1/2}$, 2.58 d; β^-, 100%; mean β^--energy, 141 keV; maximum β^--energy, 562 keV) and ^{64}Cu ($t_{1/2}$, 12.7 h), which are increasingly being exploited for their theranostics potentials. This surge is marked by recent advancements in the production of clinical-grade ^{67}Cu and its potential to be used as a theranostic single (*6,7*). The β^--emissions of ^{67}Cu have higher mean and maximal energies than those of ^{177}Lu and therefore are expected to have therapeutic effects similar to or better than those of ^{177}Lu. For SPECT imaging, ^{177}Lu (γ-energy, 208 keV [11.1%], 113 keV [6.6%]) has a less than ideal branching ratio of its γ-rays compared with ^{67}Cu (γ-energy, 93 keV [16%];

185 keV [48%]), making ^{67}Cu a better SPECT isotope and, more desirably, a theranostics single.

To improve the pharmacokinetics of octreotate, a truncated Evans blue was attached to DOTA-octreotate as a reversible albumin binder (*8*). The resulting peptide DOTA-Evans blue-TATE (EB-TATE) has improved pharmacokinetics and tumor uptake after radiolabeling with ^{177}Lu ([^{177}Lu]Lu-EB-TATE and ^{86}Y ([^{86}Y]Y-EB-TATE (*8*). Given the theranostics potential of ^{67}Cu, it was therefore of foremost importance to investigate the diagnostic and therapeutic potential of [^{67}Cu]Cu-EB-TATE (Supplemental Fig. 1; supplemental materials are available at http://jnm.snmjournals.org (*9,10*)) in SSTR2-positive NET models in vitro and in vivo. The in vivo effectiveness of [^{67}Cu]Cu-EB-TATE was compared with that of [^{177}Lu]Lu-EB-TATE, which is currently in phase I and II clinical trials (*8,11*).

MATERIALS AND METHODS

Materials

EB-TATE was obtained from Molecular Targeting Technologies Inc. through a research collaboration agreement, ^{67}Cu was purchased as electron linear accelerator–produced $^{67}CuCl_2$ [^{68}Zn(γ,p)^{67}Cu] from Canadian Isotope Innovations Corp., and ^{177}Lu was purchased as $LuCl_3$ from the McMaster Nuclear Reactor at McMaster University. The AR42J cell line was purchased from ATCC Inc., whereas the SSTR2-transfected cell lines BON1.SSTR2 and QGP1.SSTR2 were a kind donation from Carsten Grötzinger (Department of Hepatology and Gastroenterology, Charité–Universitätsmedizin Berlin) (*12*).

Ethics Statement

All animal procedures were performed in accordance with the guidelines on laboratory animal care and use of the Canadian Council on Animal Care and were approved by the Saskatchewan University Animal Care Committee (protocol 20220021).

Cell Culture, Flow Cytometry, and Xenografts

Cell culture conditions and xenograft establishment information are provided in the supplemental materials. BON1.SSTR2 and QGP1.SSTR2 cell lines were authenticated using short tandem repeat profiling (Centre for Applied Genomics, Hospital for SickKids) and had no detectable *Mycoplasma* before their use. To determine the relative overexpression of SSTR-2 in AR42J, BON1.SSTR2, and QGP1.SSTR2, flow cytometric analysis was performed (supplemental methods).

Radiolabeling of [^{67}Cu]$CuCl_2$ and [^{177}Lu]$LuCl_3$

To radiolabel EB-TATE with ^{67}Cu or ^{177}Lu, 50 μL of a 1 mg/mL solution of EB-TATE (dissolved in 150 mM ammonium acetate, pH 5.8) were added to a 1.5-mL Eppendorf tube containing [^{67}Cu]$CuCl_2$ or [^{177}Lu]$LuCl_3$ pH-adjusted with 150 mM ammonium acetate (250 MBq in 200 μL, pH 5.8). The tube was heated at 90°C for 40 min in a thermomixer. The extent of chelation of either ^{67}Cu or ^{177}Lu to EB-TATE was determined by spotting, developing 0.5 μL of the reaction volume (^{68}Ga-peptide thin-layer chromatography eluent pack; Trasis) for 5 min, and visualizing the peak using a Scan-RAM radio–thin-layer chromatography detector (LabLogic).

Radio–thin-layer chromatography yields of less than 95% led to purification using a Sep-Pak C18 1-cm^3 vac cartridge (catalog no. WAT054960; Waters), after which the Sep-Pak–purified sample was analyzed using reverse-phase C18 high-performance liquid chromatography (2796 bioseparations module, 2487 dual l absorbance detector, and XBridge C18 5-μm, 4.6 × 150 mm column; Waters).

The in vitro stability of [^{67}Cu]Cu-EB-TATE (n = 3) was determined after incubation in phosphate-buffered saline or human serum at 4°C and 37°C for 7 d, and the results were plotted using Prism (version 9; GraphPad).

Internalization

Using ^{177}Lu-DOTATATE, Tamborino et al. showed that the extent of DNA double-strand break is proportional to the proximity of the emission to the DNA (*13*). The extent of internalization of [^{67}Cu]Cu-EB-TATE into NET cell lines AR42J, BON1.SSTR2, and QGP1.SSTR2 was determined after treating the cells at 37°C (3 per concentration per temperature of incubation and per cell line) using the Nuclei EZ Prep isolation kit (catalog no. NUC201; Sigma-Aldrich) and counted on a γ-counter (Wallac Wizard 1480; PerkinElmer) as reported previously (*14*). A 4°C incubation assay was performed as a control. The extent of internalization was obtained by presenting the difference in internalization at 37°C and 4°C as a percentage of the total count rate on cells before acid wash (Supplemental Eq. 1).

In Vitro Cytotoxicity (2- and 3-Dimensional)

The in vitro cytotoxicity of [^{67}Cu]Cu-EB-TATE on monolayer (2-dimensional) and 3-dimensional spheroids using AR42J, BON1.SSTR2, and QGP1.SSTR2 cells was determined using IncuCyte S3 live-cell imaging (Sartorius Essen Bioscience) as previously described (*15*) (details in the supplemental materials).

Pharmacokinetics, Biodistribution, Dosimetry, and Micro-SPECT/CT Imaging

Pharmacokinetics was studied by injecting healthy female BALB/c mice (n = 3) with 3.9 ± 0.2 MBq (0.32 ± 0.013 nmol) of [^{67}Cu]Cu-EB-TATE through a tail vein following laboratory standard operating procedures (*14*).

Biodistribution was studied after injecting female athymic BALB/c nude mice bearing BON1.SSTR2 and QGP1.SSTR2 xenografts on either flank with 6.9 ± 1.2 MBq (0.57 ± 0.10 nmol) of [^{67}Cu]Cu-EB-TATE via a tail vein. Mice were euthanized at 1, 72, and 120 h (3 per time point) after injection, and activity in all organs was counted using a γ-counter and expressed as percentage injected activity per gram of organ (%IA/g) and %IA.

To estimate radiation dosimetry, healthy BALB/c mice (20 female and 24 male) were injected with 5.2 ± 1.1 MBq (0.43 ± 0.09 nmol) of [^{67}Cu]Cu-EB-TATE through the tail vein and euthanized at 25 min, 1 h, 6 h, 24 h, 48 h, and 72 h (3–4 per time point) after injection. The carcasses were collected and analyzed using a γ-counter, and activity was expressed as %IA/g and %IA. The mouse biodistribution (%IA/g) data were extrapolated to human data (%IA) using the formula %IA (human) = [%IA/g (mouse) × total body weight of mouse (in kg) × mass of human organ (in g)]/total body weight of human (in kg). For each organ, this was plotted against sampling time and used to estimate the residence time of the agent in the organ in MBq-h/MBq, represented by the area under the time–activity function integrated to infinity (complete decay) of the ^{67}Cu. The residence time was fitted into the OLINDA kinetics model (OLINDA/EXM, version 2.2; Hermes Medical Solutions) to generate absorbed doses in units of cGy/mCi of ^{67}Cu administered.

SPECT/CT imaging of female athymic BALB/c nude mice bearing BON1.SSTR2 and GQP1.SSTR2 xenografts was performed at 1, 6, 24, 48, and 72 h after a tail vein injection of 8.0 ± 1.4 MBq of [^{67}Cu]Cu-EB-TATE (n = 3), using a Vector4CT scanner (MILabs). The SPECT images were acquired over 35 min, whereas the CT images were acquired over 5 min. Generated CT and SPECT images were analyzed on the PMOD 3.7 software package (PMOD).

Radiotherapy

Female athymic BALB/c nude mice bearing subcutaneous BON1.SSTR2 (n = 15) and QGP1.SSTR2 (n = 16) xenografts (84.2 ± 63.3 mm^3) were allocated to 3 groups (5 or 6/group) per

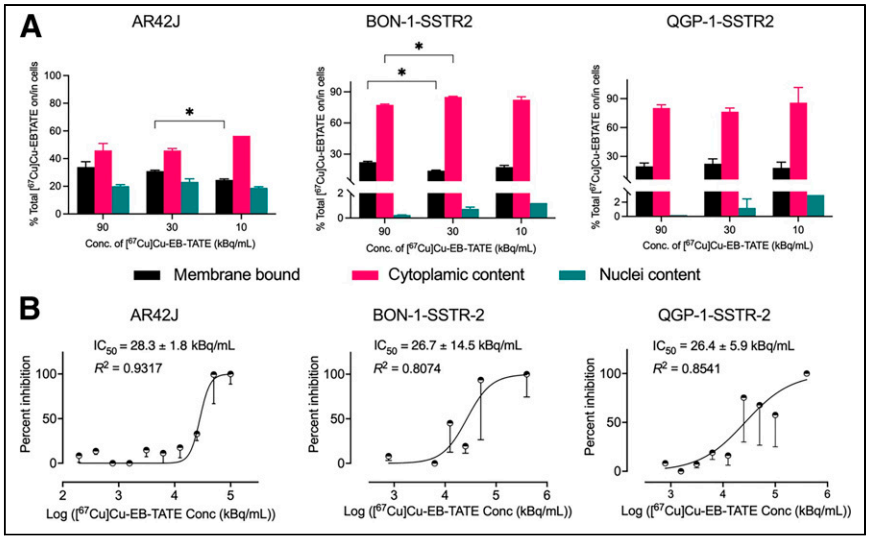

FIGURE 1. Internalization and in vitro cytotoxicity of [^{67}Cu]Cu-EB-TATE in NET cell lines with different SSTR2 densities. (A) Internalization after 2.5 h of incubation at different concentrations of [^{67}Cu]Cu-EB-TATE. (B) In vitro cytotoxicity in 2-dimensional monolayer of NET cell lines using live cell imaging. IC_{50} = 50% inhibitory concentration. *$P < 0.0332$.

xenograft model, each receiving the vehicle (saline), 2 doses of 15 MBq (10 d apart) of [^{67}Cu]Cu-EB-TATE in saline, or 2 doses of 15 MBq (10 d apart) of [^{177}Lu]Lu-EB-TATE in saline, via a tail vein in a final volume of 100 μL. The mice were monitored daily for general health status, and tumor and body weight were measured 3 times a week. The tumor size endpoint for euthanasia was 1,500 mm^3. Tumor size was measured using a digital caliper, and volume was determined using the formula [length × width^2]/2.

Statistical Analysis

All results are presented as mean ± SD, except when otherwise stated as the mean ± SEM of at least 3 replicated experiments. Percentage tumor growth inhibition of test groups was determined relative to control groups using the formula $[1 - \Delta T/\Delta C] \times 100$, where ΔT and ΔC are the differences between the final and initial tumor volumes of the test and control groups, respectively. Statistical analysis was performed using GraphPad Prism 9. ANOVA was performed on the slope parameters of spheroid growth, followed by the Dunnett post hoc test to compare treatment groups.

RESULTS

Radiolabeling and In Vitro Stability

The best specific activity of [^{67}Cu]Cu-EB-TATE was found to be 5 MBq/μg of peptide, with a resulting radiochemical yield of 95% by instant thin-layer chromatography, whereas radiolabeling of [^{177}Lu]Lu-EB-TATE at this specific activity resulted in a radiochemical yield of 90% (Supplemental Figs. 2A and 2B). Radiochemical purity as shown by reverse-phase C18 high-performance liquid chromatography was at least 98% (Supplemental Fig. 3). The in vitro stability of [^{67}Cu]Cu-EB-TATE was determined in phosphate-buffered saline at 4°C and in human serum at 37°C for 7 d. Average daily yields of intact [^{67}Cu]Cu-EB-TATE, normalized to the initial yield on day 0 as 100%, showed that [^{67}Cu]Cu-EB-TATE was more than 91% stable on day 6 in both human serum and phosphate-buffered saline (Supplemental Fig. 4).

Overexpression of SSTR-2 in NET Cell Lines

Flow cytometry using phycoerythrin-conjugated anti-SSTR2 showed that QGP1.SSTR2 has an increased expression of SSTR2 compared with standard high-expressing AR42J, which has similar expression levels to BON1.SSTR2 (Supplemental Figs. 5 and 6).

Internalization of [^{67}Cu]Cu-EB-TATE and Cytotoxicity Against NET Cell Lines In Vitro

The internalization of [^{67}Cu]Cu-EB-TATE was studied in AR42J, BON1.SSTR2, and QGP1.SSTR2 cell lines. After 2.5 h of incubation followed by compartmental internalization analyses, the total internalization fraction (nuclei plus cytoplasmic) at 90 kBq/mL was observed to increase slightly, though not significantly, from 66.1% ± 5.4% (AR42J) to 78.6 ± 1.2 (BON1.SSTR22, $P = 0.0834$) and to 80.4 ± 3.5 (QGP1.SSTR2, $P = 0.0898$). Moreover, no differences were seen in total internalization for a given cell line across the 3 tested concentrations except for AR42J (at 30 kBq/mL and 10 kBq/mL) and BON1.SSTR2 (90 kBq/mL and 30 kBq/mL) (Fig. 1A).

The concentration of [^{67}Cu]Cu-EB-TATE that inhibited 50% of NET cells AR42J, BON1.SSTR2, and QGP1.SSTR2 in vitro after 72 h of treatment was determined and presented as mean ± SEM. There were no significant differences in the 50% inhibitory concentrations for AR42J (28.3 ± 1.8 kBq/mL), BON1.SSTR2 (26.7 ± 14.5 kBq/mL), or QGP1.SSTR2 (26.4 ± 5.9 kBq/mL) (Fig. 1B).

To further evaluate the cytotoxicity of [^{67}Cu]Cu-EB-TATE in vitro, spheroid models of BON1.SSTR2 and QGP1.SSTR2 were developed. [^{67}Cu]Cu-EB-TATE at activity concentrations of at least 8 kBq/mL inhibited the growth of QGP1.SSTR2 spheroids but not the growth of BON1.SSTR2 spheroids (Supplemental Figs. 7A and 7B). At 150 h after treatment, QGP1.SSTR2 spheroids' size decreased from 0.57 ± 0.04 mm^2 to 0.54 ± 0.02 mm^2 ($P = 0.0002$)

TABLE 1
Pharmacokinetics of [^{67}Cu]Cu-EB-TATE in Healthy Female BALB/c Mice

Pharmacokinetic parameter	Data
Area under curve (%IA·h/mL)	634.9 ± 6.9
Distribution $t_{1/2}$ (h)	0.6 ± 0.1
Clearance $t_{1/2}$ (h)	33.5 ± 5.2
Elimination constant (h^{-1})	0.13 ± 0.01
Volume at steady-state (mL)	6.9 ± 1.1
Clearance rate (mL/h)	0.16 ± 0.00

Data are mean ± SD. Mice were injected with 3.86 ± 0.16 MBq (0.32 ± 0.013 nmol) of [^{67}Cu]Cu-EB-TATE, and values were obtained from %IA/mL and time (h).

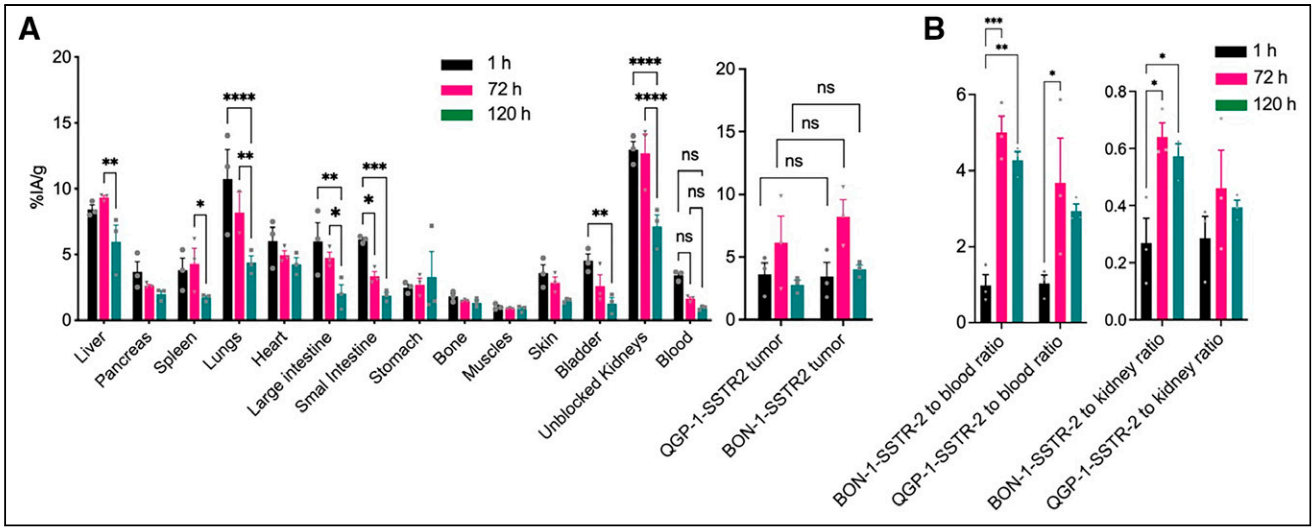

FIGURE 2. Ex vivo biodistribution of [^{67}Cu]Cu-EB-TATE in athymic nude mice bearing QGP1.SSTR2 and BON1.SSTR2 xenografts. (A) Retention of [^{67}Cu]Cu-EB-TATE in tumors and blood, accompanied by clearance from major organs. (B) Increase in tumor-to-blood and tumor-to-kidney ratios over time. ns = no significance. *$P \leq 0.0332$. **$P \leq 0.0021$. ***$P \leq 0.00002$. ****$P \leq 0.0001$.

and $0.48 \pm 0.0.03$ mm^2 ($P < 0.0001$) at 200 kBq/mL, and 1,000 kBq/mL, respectively, against 0.62 ± 0.04 mm^2 for control spheroids. For BON1.SSTR2, spheroid growth changed from 0.74 ± 0.04 mm^2 to 0.94 ± 0.06 mm^2 ($P = 0.1766$) and 0.89 ± 0.03 mm^2 ($P = 0.0953$) at 200 kBq/mL and 1,000 kBq/mL, respectively, against 1.01 ± 0.09 mm^2 for control.

Similarly, spheroid death as indicated by red object count (per image) increased with time and with activity concentration of [^{67}Cu]Cu-EB-TATE in both spheroid models (Supplemental Fig. 7C).

Pharmacokinetics, Biodistribution, Micro-SPECT/CT Imaging, and Dosimetry

In healthy female BALB/c mice, [^{67}Cu]Cu-EB-TATE exhibited a biphasic $t_{1/2}$ with a fast distribution and slow clearance phase (Table 1; Supplemental Fig. 8). Athymic BALB/c nude mice bearing a QGP1.SSTR2 xenograft on the right flank and a BON1.SSTR2 xenograft on the left flank were injected with [^{67}Cu]Cu-EB-TATE through a tail vein. Ex vivo biodistribution, reported as %IA/g at 1, 72, and 120 h after injection, showed a clear trend in clearance from major tissues except the tumor, where retention was well evident (Fig. 2A). Uptake of [^{67}Cu]Cu-EB-TATE in QGP1.SSTR2 and BON1.SSTR2 xenografts was similar (P values for 1, 72, and 120 h being 0.9910, 0.7148, and 0.1347, respectively) (Fig. 2A). Analyses of tumor-to-blood and tumor-to-kidney ratios are also shown (Fig. 2B).

Micro-SPECT/CT images showed high bladder uptake at 1 h after injection (4.5 ± 0.1%IA/g) but not at later times. The kinetics of distribution of [^{67}Cu]Cu-EB-TATE in organs and tumors clearly showed clearance from all organs except the tumors, where there was accumulation (Fig. 3). Images acquired from another mouse with a bigger QGP1.SSTR2 xenograft showed little uptake in the kidneys and livers, compared with the tumor at 72 h after injection (Supplemental Fig. 9).

Organ dose estimation after an intravenous injection of 5.22 ± 1.11 MBq of [^{67}Cu]Cu-EB-TATE in healthy BALB/c male and female mice (3–4 per sex per time point) was performed using %IA/g data for 5 time points between 1 and 72 h (Supplemental Table 1). Projected human absorbed doses (mSv/MBq) for organs, and effective and total-body dose, are presented (Table 2). In female mice, the organs with the highest dose (in decreasing order) were kidneys > lungs > liver > heart > pancreas > spleen, whereas for males, the order was liver > lungs > spleen > pancreas.

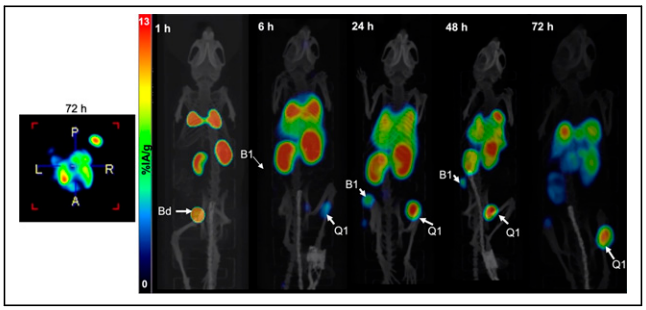

FIGURE 3. Kinetics of [^{67}Cu]Cu-EB-TATE uptake using micro-SPECT/CT. Maximum-intensity projection micro-SPECT/CT image of mouse injected with 6.45 MBq (0.53 nmol) of [^{67}Cu]Cu-EB-TATE shows accumulation and retention of theranostic in tumors and clearance from healthy organs. A = anterior; B1 = BON1.SSTR2 xenograft; Bd = bladder; P = posterior; Q1 = QGP1.SSTR2 xenograft.

Efficacy of [^{67}Cu]Cu-EB-TATE in Mouse Xenografts

Athymic BALB/c nude mice bearing either BON1.SSTR2 or QGP1.SSTR2 xenografts were treated using 2 doses of either [^{67}Cu]Cu-EB-TATE or [^{177}Lu]Lu-EB-TATE (administered 10 d apart) or vehicle (saline) as control. Tumor volumes between groups at the start of treatment were statistically similar except for QGP1.SST2 saline-treated versus QGP1.SSTR2 [^{177}Lu]Lu-EB-TATE–treated ($P = 0.0428$) (Supplemental Tables 2A and 2B). [^{67}Cu]Cu-EB-TATE was effective against BON1.SSTR2 and QGP1.SSTR2 xenografts, with results comparable to [^{177}Lu]Lu-EB-TATE. Moreover, treatment with 15 MBq of [^{67}Cu]Cu-EB-TATE or [^{177}Lu]Lu-EB-TATE, administered 10 d apart, was tolerated by athymic BALB/c nude mice as indicated by body weight (Figs. 4 and 5).

For QGP1.SSTR2 therapy (Fig. 4A), the [^{67}Cu]Cu-EB-TATE treatment group had 90.3% tumor inhibition by day 15 compared

TABLE 2
Projected Human Absorbed Doses of [^{67}Cu]Cu-EB-TATE

Organ	Absorbed dose (mSv/MBq)	
	Female	Male
Adrenals	3.54E−02	2.10E−02
Brain	1.69E−02	1.90E−02
Breast	5.28E−03	
Esophagus	2.09E−02	1.62E−02
Eyes	9.28E−04	7.67E−04
Gallbladder	2.29E−02	2.81E−02
Left colon	1.59E−01	1.52E−01
Small intestine	6.93E−03	9.56E−02
Stomach	1.40E−02	3.40E−02
Right colon	7.30E−03	8.86E−03
Rectum	1.27E−03	1.86E−03
Heart wall	1.93E−01	1.27E−01
Kidneys	6.02E−01	1.03E−02
Liver	3.42E−01	3.09E−01
Lungs	3.91E−01	2.88E−01
Ovaries	1.81E−03	
Pancreas	1.61E−01	1.07E−01
Prostate		1.60E−03
Salivary glands	1.47E−03	1.20E−03
Red marrow	8.54E−03	6.08E−03
Osteogenic cells	1.35E−02	9.26E−03
Spleen	1.41E−01	1.19E−01
Testes		1.53E−04
Thymus	1.81E−02	1.10E−02
Thyroid	7.37E−03	6.41E−03
Bladder	1.21E−02	1.47E−02
Uterus	1.73E−03	
Total body	2.34E−02	1.59E−02
Effective dose	8.50E−02	6.61E−02

with the [^{177}Lu]Lu-EB-TATE treatment group, which had 70.2% tumor inhibition. By day 90, 2 of 5 mice in the [^{67}Cu]Cu-EB-TATE treatment group had complete remission, compared with 1 of 5 mice with complete remission in the [^{177}Lu]Lu-EB-TATE treatment group. The median survival (1,500 mm^3 study endpoint) of the saline group was 26 d, compared with 90 d for the [^{67}Cu]Cu-EB-TATE group. At 90 d after treatment, median survival for the [^{177}Lu]Lu-EB-TATE–treated mice had not been reached (Fig. 4B). Interestingly, [^{67}Cu]Cu-EB-TATE was better tolerated than [^{177}Lu]Lu-EB-TATE as shown by the slope of body weights ($P < 0.0001$) (Fig. 4C).

For BON1.SSTR2, both [^{67}Cu]Cu-EB-TATE and [^{177}Lu]Lu-EB-TATE treatments showed similar effectiveness (Fig. 5A). By day 26 after the start of treatment, the [^{67}Cu]Cu-EB-TATE treatment group had a tumor inhibition of 95.4%, which was similar to that of the [^{177}Lu]Lu-EB-TATE treatment group, at 92.7% inhibition. By day 90, 1 of 5 mice in both the [^{67}Cu]Cu-EB-TATE treatment group and the [^{177}Lu]Lu-EB-TATE treatment group had complete remission. The median survival (1,500 mm^3 study endpoint) of the saline group was 53 d, whereas that for the [^{67}Cu]Cu-EB-TATE treatment group was not reached by day 90. In comparison, median survival for the [^{177}Lu]Lu-EB-TATE–treated group was 89 d (Fig. 5B). Tolerance to treatments as indicated by body weight was similar (slopes, $P = 0.1368$) (Fig. 5C).

DISCUSSION

Given the unique theranostic properties of ^{67}Cu as a single agent or in combination with ^{64}Cu (*16,17*), and considering the recent advances in ^{67}Cu production (*6*), this study was aimed to investigate the theranostic properties of [^{67}Cu]Cu-EB-TATE against SSTR2-positive NETs. Previous preclinical NET studies on peptide receptor radionuclide therapy have used SSTR2 transduced or transfected cell lines such as the human non–small lung cancer cell line A-427 (*18*), the human primary pancreatic tumor cell line QGP, and the human metastatic peripancreatic cell line BON1 (*19,20*) or endogenous SSTR2-expressing cell lines such as the rat pancreatic neuroendocrine cell line AR42J (*7,11*). Here, SSTR2-transfected BON1 (BON1.SSTR2) and QGP1 (QGP1.SSTR2) with clinically relevant levels of receptor expression were used. In vitro internalization and cytotoxicity studies were performed to prevalidate these NET cell lines for therapy studies using [^{67}Cu]Cu-EB-TATE (Fig. 1; Supplemental Figs. 5–7).

Initially, we looked to show that [^{67}Cu]Cu-EB-TATE had similar pharmacologic properties to [^{177}Lu]Lu-EB-TATE. To this end,

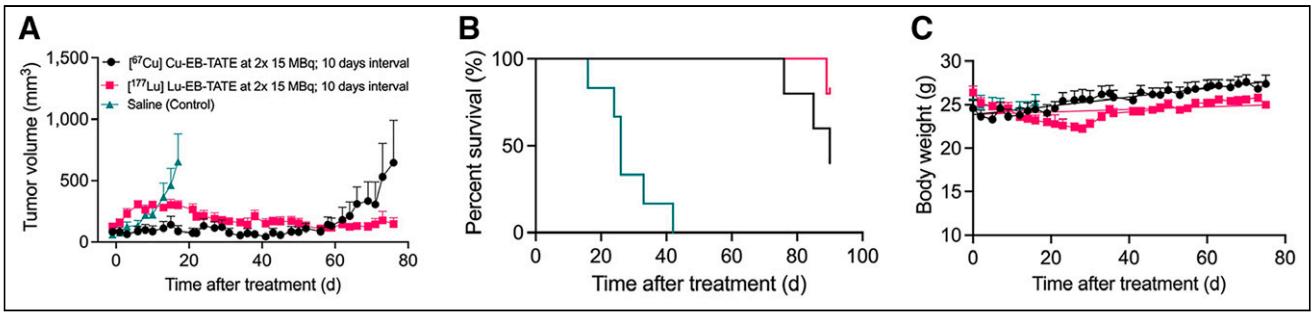

FIGURE 4. Efficacy of [^{67}Cu]Cu-EB-TATE against SSTR2-positive QGP1.SSTR2 xenograft. QGP1.SSTR2 tumor–bearing athymic BALB/c nude mice (5 or 6/group) were injected with 15 MBq of either [^{67}Cu]Cu-EB-TATE or [^{177}Lu]Lu-EB-TATE on days 0 and 10. Control mice were injected with vehicle (saline) on day 0. Tumors were measured 3 times per week and plotted against days after treatment (A). Percentage survival was also plotted (B), and body weight was monitored for entire duration of study (90 d) (C). Plots were discontinued when tumor volume of mouse in particular group reached 1,500 mm^3. Survival was defined as time to reach tumor volume ≥ 1,500 mm^3 or time of 90 d.

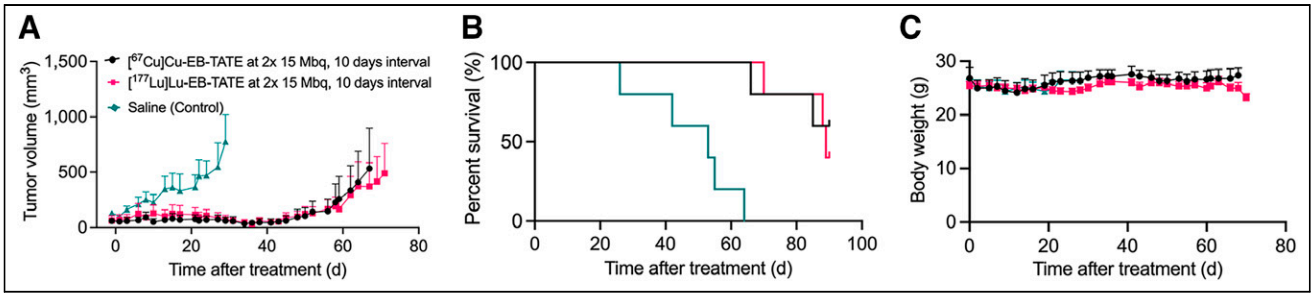

FIGURE 5. Efficacy of [^{67}Cu]Cu-EB-TATE against BON1.SSTR2 xenograft. BON1.SSTR2 tumor–bearing athymic BALB/c nude mice (n = 5/group) were injected with 15 MBq of either [^{67}Cu]Cu-EB-TATE or [^{177}Lu]Lu-EB-TATE on days 0 and 10. Control mice were injected with vehicle (saline) on day 0. Tumors were measured 3 times per week and plotted against days after treatment (A). Percentage survival was also plotted (B), and body weight was monitored for entire duration of study (90 d) (C). Plots were discontinued when tumor volume of mouse in particular group reached 1,500 mm$^{3.}$ Survival was defined as time to reach tumor volume ≥ 1,500 mm^3 or time of 90 d.

we studied the pharmacokinetics and dosimetry of [^{67}Cu]Cu-EB-TATE in healthy BALB/c mice and confirmed that [^{67}Cu]Cu-EB-TATE had prolonged circulation (distribution $t_{1/2}$, 0.6 ± 0.1 h; clearance $t_{1/2}$, 33.5 ± 5.2 h) (Table 1). Blood distribution of [^{177}Lu]Lu-EB-TATE in human NET patients has been similarly reported, with prolonged clearance (distribution $t_{1/2}$, 9.47 h; clearance $t_{1/2}$, 236 h) (*21*). The projected human dose of [^{67}Cu]Cu-EB-TATE in the kidneys (unblocked) as obtained in this study (female, 0.60 mSv/MBq; male, 0.01 mSv/MBq) (Table 2) is less than the actual kidney dose in NET patients for [^{177}Lu]Lu-EB-TATE (1.15 mSv/MBq) but similar to [^{177}Lu]Lu-DOTATATE (0.36 mSv/MBq) (*21*). Interestingly, the projected human effective dose for [^{67}Cu]Cu-EB-TATE in male patients (0.066 mSv/MBq) is less than that in female patients (0.085 mSv/MBq) and that for [^{177}Lu]Lu-EB-TATE (0.080 mSv/MBq) but similar to that for [^{177}Lu]Lu-DOTATATE (0.069 mSv/MBq) (*21*). The reported kidney dose for [^{64}Cu]Cu-SarTATE has been similar (0.20 mSv/MBq), with an effective dose of 0.045 mSv/MBq (*22*).

The ex vivo biodistribution of [^{67}Cu]Cu-EB-TATE was studied in athymic nude mice bearing both QGP1.SSTR2 and BON1.SSTR2 xenografts. Prolonged accumulation was observed in tumors (Fig. 2A), peaking at 72 h after injection [QGP1.SSTR2, 8.2 ± 2.4%IA/g [P = 0.4206, not statistically significant]; BON1.SSTR2, 6.1 ± 3.7%IA/g [P = 0.0474]) from 1 h. Tian et al. earlier reported a similar tumor accumulation of ^{86}Y-EB-TATE at 48 h after injection (*8*) in a HCT116.SSTR2 xenograft model. Therefore, tumor uptake in this study was similar to what was observed with other radiometals. Confirmatively, acquired micro-SPECT/CT images of [^{67}Cu]Cu-EB-TATE (Fig. 3) showed specific binding and high retention in NET tumors, with clearance from healthy organs. Conversely, [^{177}Lu]Lu-DOTATATE tumor uptake peaked at 1 h because of fast blood clearance (*23*). This translates to a higher-activity injection of DOTATATE to attain dose levels similar to EB-TATE peptide.

QGP1.SSTR2 tumor–bearing mice and BON1.SSTR2 tumor–bearing mice were treated using [^{67}Cu]Cu-EB-TATE, [^{177}Lu]Lu-EB-TATE, or saline. [^{67}Cu]Cu-EB-TATE and [^{177}Lu]Lu-EB-TATE were both efficacious against the 2 tumor models. Interesting, [^{67}Cu]Cu-EB-TATE appeared (not statistically significantly) to be more efficacious at eliminating QGP1.SSTR2 tumors (complete remission in 2/5) than was [^{177}Lu]Lu-EB-TATE (complete remission in 1/5), though with a shorter average tumor growth delay (Figs. 4A and 5A). The 90-d median survival was prolonged, against saline control, for [^{67}Cu]Cu-EB-TATE–treated mice (QGP1.SSTR2, 90 d; BON1.SSTR2, not reached) (log-rank $P < 0.0001$) and [^{177}Lu]Lu-EB-TATE–treated mice (QGP1.SSTR2, not reached; BON1.SSTR2, 89 d) (Figs. 4B and 5B). This survival is better than that in a 100-d study whose median survival for [^{225}Ac]Ac-MACROPATATE (an octreotide derivative labeled with ^{225}Ac via an 18-membered macrocyclic chelator macropa) was 55 d, versus 26 d for saline control, in an H68 NET xenograft model. Similarly, [^{225}Ac]Ac-MACROPATATE was not as effective as [^{225}Ac]Ac-DOTATATE, with 80% (8/10) survival at 100 d (*24*). The efficacies and tolerance displayed by [^{67}Cu]Cu-EB-TATE and [^{177}Lu]Lu-EB-TATE were similar. Given its superior image quality, [^{67}Cu]Cu-EB-TATE can be used to estimate organ dosimetry and to treat and monitor treatment of SSTR2-positive tumors. In a PET/CT setting, [^{64}Cu]Cu-EB-TATE diagnostic PET images could be of added value given the inherent resolution of the modality. Given the recent increased availability of high-specific-activity [^{67}Cu]Cu and [^{64}Cu]Cu, these theranostics have tremendous potential for the management of NETs.

CONCLUSION

As rationalized, the therapeutic potential of [^{67}Cu]Cu-EB-TATE was similar to that of [^{177}Lu]Lu-EB-TATE. In addition, [^{67}Cu]Cu-EB-TATE exhibited excellent SPECT/CT imaging capabilities even at 96 h after injection, which would in theory allow for better sensitivity and tumor delineation, particularly for lesions in organs that have a high blood pool and cannot be delineated using ^{68}Ga tracers. It would also allow for increased accuracy in dosimetry estimation compared with situations in which other surrogate radionuclides are used. [^{67}Cu]Cu-EB-TATE therefore warrants clinical investigation as a theranostic.

DISCLOSURE

This work was realized with funding from the Sylvia Fedoruk Centre for Nuclear Innovation (grant J2018-0042). Koon Pak and Brian Gray are employees and shareholders of Molecular Targeting Technologies Inc., which has an exclusive license from the National Institutes of Health for EB-TATE. No other potential conflict of interest relevant to this article was reported.

ACKNOWLEDGMENTS

We appreciate Dr. Carsten Grötzinger for providing us with SSTR2-transfected QGP1.SSTR2 and BON1.SSTR2 cell lines. We thank Dr. Vijay Gaja of the Canadian Isotope Innovations Corp. for providing us with ^{67}Cu.

KEY POINTS

QUESTION: Is [^{67}Cu]Cu-EB-TATE an effective theranostic for the management of SSTR2-expressing NETs, and what possible edge does it present over [^{177}Lu]Lu-EB-TATE peptide receptor radionuclide therapy?

PERTINENT FINDINGS: In vivo tumor uptake and retention of [^{67}Cu]Cu-EB-TATE was excellent, giving it great dosimetry estimation and SPECT imaging capabilities. [^{67}Cu]Cu-EB-TATE was effective against SSTR2-positive neuroendocrine xenografts. Moreover, it appeared to be very effective in eliminating small-volume tumors.

IMPLICATIONS FOR PATIENT CARE: [^{67}Cu]Cu-EB-TATE has the potential for SPECT imaging, dosimetry, and treatment of NET tumors, particularly for the elimination of small-volume metastasis.

REFERENCES

1. Barakat MT, Meeran K, Bloom SR. Neuroendocrine tumours. *Endocr Relat Cancer.* 2004;11:1–18.
2. Patel P, Galoian K. Molecular challenges of neuroendocrine tumors. *Oncol Lett.* 2018;15:2715–2725.
3. Tsoli M, Chatzellis E, Koumarianou A, Kolomodi D, Kaltsas G. Current best practice in the management of neuroendocrine tumors. *Ther Adv Endocrinol Metab.* 2019;10:2042018818804698.
4. Hennrich U, Kopka K. Lutathera®: the first FDA- and EMA-approved radiopharmaceutical for peptide receptor radionuclide therapy. *Pharmaceuticals (Basel).* 2019;12:114.
5. Deppen SA, Liu E, Blume JD, et al. Safety and efficacy of ^{68}Ga-DOTATATE PET/CT for diagnosis, staging, and treatment management of neuroendocrine tumors. *J Nucl Med.* 2016;57:708–714.
6. Mou L, Martini P, Pupillo G, Cieszykowska I, Cutler CS, Mikolajczak R. ^{67}Cu production capabilities: a mini review. *Molecules.* 2022;27:1501.
7. Cullinane C, Jeffery CM, Roselt PD, et al. Peptide receptor radionuclide therapy with ^{67}Cu-CuSarTATE is highly efficacious against a somatostatin-positive neuroendocrine tumor model. *J Nucl Med.* 2020;61:1800–1805.
8. Tian R, Jacobson O, Niu G, et al. Evans blue attachment enhances somatostatin receptor subtype-2 imaging and radiotherapy. *Theranostics.* 2018;8:735–745.
9. Luley KB, Biedermann SB, Kunstner A, et al. A comprehensive molecular characterization of the pancreatic neuroendocrine tumor cell lines BON-1 and QGP-1. *Cancers (Basel).* 2020;12:691.
10. Vandamme T, Peeters M, Dogan F, et al. Whole-exome characterization of pancreatic neuroendocrine tumor cell lines BON-1 and QGP-1. *J Mol Endocrinol.* 2015;54:137–147.
11. Thakur S, Daley B, Millo C, et al. ^{177}Lu-DOTA-EB-TATE, a radiolabeled analogue of somatostatin receptor type 2, for the imaging and treatment of thyroid cancer. *Clin Cancer Res.* 2021;27:1399–1409.
12. Exner S, Prasad V, Wiedenmann B, Grotzinger C. Octreotide does not inhibit proliferation in five neuroendocrine tumor cell lines. *Front Endocrinol (Lausanne).* 2018;9:146.
13. Tamborino G, Perrot Y, De Saint-Hubert M, et al. Modeling early radiation DNA damage occurring during ^{177}Lu-DOTATATE radionuclide therapy. *J Nucl Med.* 2022;63:761–769.
14. Hartimath SV, Alizadeh E, Solomon VR, et al. Preclinical evaluation of ^{111}In-labeled PEGylated maytansine nimotuzumab drug conjugates in EGFR-positive cancer models. *J Nucl Med.* 2019;60:1103–1110.
15. Tikum AF, Nambisan AK, Ketchemen JP, et al. Simultaneous imaging and therapy using epitope-specific anti-epidermal growth factor receptor (EGFR) antibody conjugates. *Pharmaceutics.* 2022;14:1917.
16. Loft M, Carlsen EA, Johnbeck CB, et al. ^{64}Cu-DOTATATE PET in patients with neuroendocrine neoplasms: prospective, head-to-head comparison of imaging at 1 hour and 3 hours after injection. *J Nucl Med.* 2021;62:73–80.
17. Hao G, Mastren T, Silvers W, Hassan G, Oz OK, Sun X. Copper-67 radioimmunotheranostics for simultaneous immunotherapy and immuno-SPECT. *Sci Rep.* 2021;11:3622.
18. Parry JJ, Eiblmaier M, Andrews R, et al. Characterization of somatostatin receptor subtype 2 expression in stably transfected A-427 human cancer cells. *Mol Imaging.* 2007;6:56–67.
19. Guenter R, Aweda T, Carmona Matos DM, et al. Overexpression of somatostatin receptor type 2 in neuroendocrine tumors for improved Ga68-DOTATATE imaging and treatment. *Surgery.* 2020;167:189–196.
20. Jin XF, Auernhammer CJ, Ilhan H, et al. Combination of 5-fluorouracil with epigenetic modifiers induces radiosensitization, somatostatin receptor 2 expression, and radioligand binding in neuroendocrine tumor cells in vitro. *J Nucl Med.* 2019;60:1240–1246.
21. Zhang J, Wang H, Jacobson O, et al. Safety, pharmacokinetics, and dosimetry of a long-acting radiolabeled somatostatin analog ^{177}Lu-DOTA-EB-TATE in patients with advanced metastatic neuroendocrine tumors. *J Nucl Med.* 2018;59:1699–1705.
22. Hicks RJ, Jackson P, Kong G, et al. ^{64}Cu-SARTATE PET imaging of patients with neuroendocrine tumors demonstrates high tumor uptake and retention, potentially allowing prospective dosimetry for peptide receptor radionuclide therapy. *J Nucl Med.* 2019;60:777–785.
23. Liu F, Zhu H, Yu J, et al. ^{68}Ga/^{177}Lu-labeled DOTA-TATE shows similar imaging and biodistribution in neuroendocrine tumor model. *Tumour Biol.* 2017;39:1010428317705519.
24. King AP, Gutsche NT, Raju N, et al. ^{225}Ac-MACROPATATE: a novel alpha-particle peptide receptor radionuclide therapy for neuroendocrine tumors. *J Nucl Med.* 2023;64:549–554.